Optical trapping and spectral analysis of aerosols with a supercontiuum laser source

M. Guillon[1], K. Dholakia[2] and D. McGloin[1]

[1]*Electronic Engineering and Physics, University of Dundee, Nethergate, Dundee, UK DD1 4HN.*
[2]*SUPA, School of Physics and Astronomy, University of St. Andrews, North Haugh, Fife, Scotland, UK KY16 9SS.*

m.guillon@dundee.ac.uk

http://www.dundee.ac.uk/elecengphysics/tweezers/index.htm

Abstract: We report on the optical trapping of water droplets with a supercontinuum laser source. Droplet size is determined by observing the spectrum of the on-axis backscattered light. In contrast to to monochromatic trapping, the broad spectrum of the supercontinuum covers several resonances of the first excited Mie coefficients. A minimum value of $Q \sim 0.16$ for the trapping efficiency is estimated.

© 2008 Optical Society of America

OCIS codes: (140.7010) Lasers and laser optics: Laser Trapping; (350.4855) Optical tweezers or optical manipulation; (010.1110) Aerosols

References and links

1. D. McGloin, "Optical Tweezers: 20 years on," Philos. Trans. Roy. Soc. A **364** 3521-3527 (2006)
2. K. Dholakia, P. Reece and M. Gu, "Optical micromanipulation," Chem. Soc. Rev. **37,** 42-55 (2008)
3. N. Magome, M. I. Kohira, E. Hayata, S. Mukai and K. Yoshikawa, "Optical trapping of a growing water droplet in air," J. Phys. Chem. B **107,** 3988-3990 (2003)
4. R. J. Hopkins, L. Mitchem, A. D. Ward, and J. P. Reid, "Control and characterisation of a single aerosol droplet in a single beam gradient force optical trap," Phys. Chem. Chem. Phys. **6,** 4924-4927 (2004).
5. D. R. Burnham and D. McGloin, "Holographic optical trapping of aerosol droplets," Opt. Express, **14** 4175-4181 (2006)
6. M. D. King, K. C. Thompson, and A. D. Ward, "Laser tweezers Raman study of optically trapped aerosol droplets of Seawater and oleic acid reacting with ozone: Implications for cloud-droplet properties," JACS **126** 16710-16711 (2004)
7. J. Buajarern, L. Mitchem, and J. P. Reid, "Manipulation and characterization of aqueous sodium dodecyl sulfate/sodium chloride aerosol particles," J. Phys. Chem. A **111** 13038-13045 (2007)
8. J. Buajarern, L. Mitchem, and J. P. Reid, "Characterizing multiphase Organic/Inorganic/Aqueous aerosol droplets," J. Phys. Chem. A, **111** 9054-9061 (2007)
9. R. Leonardo, *et al.*, "Parametric resonance of optically trapped aerosols," Phys. Rev. Lett. **99** 010601 (2007)
10. R. R. Alfano, ed., The Supercontinuum Laser Source, Sec. Edition, (Springer, New York, 2006).
11. P. Li, K. Shi, and Z. Liu, "Manipulation and spectroscopy of a single particle by use of white-light optical tweezers," Opt. Lett. **30,** 156-158 (2005).
12. P. Fischer, A. E. Carruthers, K. Volke-Sepulveda, E. M. Wright, C. T. A. Brown, W. Sibbett and K. Dholakia, "Enhanced optical guiding of colloidal particles using a supercontinuum light source," Opt. Express, **14** 5792-5802 (2006)
13. M. Guillon, "Field enhancement in a chain of optically bound dipoles," Opt. Express **14,** 3045-3055 (2006).
14. J. Buajarern, L. Mitchem, A. D. Ward, N. Hendrik Nahler, D. McGloin, and J. P. Reid, "Controlling and Characterising the Coagulation of Liquid Aerosol Droplets," J. Chem. Phys. **125,** 114506 (2006).
15. A. Ashkin and J. M. Dziedzic, "Observation of optical resonances of dielectric spheres by light scattering," Appl. Opt. **20,**, 1803-1814 (1981).

16. A. Mazolli, P. A. Maia Neto, and H. M. Nussenzveig,"Theory of trapping forces in optical tweezers," Proc. R. Soc. Lond. A **459**, 3021-3041 (2003).
17. O. Moine and B. Stout, "Optical force calculations inarbitrary beams by the use of the vector addition theorem," J. Opt. Soc. Am. B **22**, 1620-1631 (2005).
18. P. Chylek, V. Ramaswamy, A. Ashkin, and J. M. Dziedzic, "Simultaneous determination of refractive index and size of spherical dielectric particles from light scattering data," Appl. Opt. **22**, 2302-2307 (1983).
19. C. C. Lam, P. T. Leung, and K. Young, "Explicit asymptotic formulas for the positions, widths, and strengths of resonances in Mie scattering," J. Opt. Soc. Am. B **9,** 1585-1592 (1992).
20. S. Schiller and R. L. Byer, "High-resolution spectroscopy of whispering gallery modes in large dielectric spheres," Opt. Lett. **16,** 1138-1140 (1991).
21. M. Guillon and B. Stout, "Optical trapping and binding in air: imaging and spectroscopic analysis," Phys. Rev. A **77,** 023806 (2008).
22. D. McGloin, D. R. Burnham, M. D. Summers, D. Rudd, N. Dewar, and S. Anand, "Optical manipulation of airborne particles: techniques and applications," Faraday Discuss. **137,** 335-350 (2008).
23. A. Ashkin and J. M. Dziedzic, "Optical levitation in high vacuum," Appl. Phys. Lett. **28,**, 333-335 (1976).
24. D. R. Burnham and D. McGloin, manuscript in preparation
25. A. Ashkin, "Forces of a single-beam gradient laser trap on a dielectric sphere in the ray optics regime," Biophys. J. **61,** 569-582 (1992).
26. A. Ashkin and J. M. Dziedzic, "Observation of Resonances in the Radiation Pressure on Dielectric Spheres," Phys. Rev. Lett. **38,** 1351-1354 (1977).
27. J. R. Butler, L. Mitchem, K. L. Hanford, L. Treuelb, and J. P. Reid, "In situ comparative measurements of the properties of aerosol droplets of different chemical composition," Faraday Discuss. **137** 351-366 (2008).
28. P. Török, P. Varga, Z. Laczik, and G. R. Booker, "Electromagnetic diffraction of light focused through a planar interface between materials of mismatched refractive indices: an integral representation, " J. Opt. Soc. Am. A **12,** 325-332 (1995).
29. D. A. Varshalovich, A. M. Moskalev, and V. K. Khersonskii, Quantum theory of angular momentum, (World Scientific, Singapor, 1988), 1st edition, ISBN 9971-50-107-4.
30. C. F. Bohren and D. R. Huffman, Absorption and scattering of light by small particles, (John Willey, New York, 1983) Chap. 4.
31. P. A. Maia Neto and H. M. Nussenzveig, "Theory of optical tweezers," Europhys. Lett. **50,** 702-708 (2000).

1. Introduction

Optical trapping is a powerful tool for the manipulation of micron and submicron sized dielectric particles. The application areas of this technique are wide and interdisciplinary [1, 2]. In recent years, a growing body of work has developed in airborne optical trapping [3], in particular liquid aerosols [4, 5, 6, 7, 8, 9]. This work is of particular interest for the characterization of aerosols as it gives unprecedented control over single and multiple aerosol droplets and their interaction with their environment. Furthermore it allows the droplets to be controllably probed as they undergo chemical, thermodynamic and kinetic changes.

One of the most exciting developments in nonlinear optics in recent years has been the production of supercontinuum light sources [10], which have a large bandwidth (and low temporal coherence) whilst retaining a high spatial coherence. The large spectrum of these sources is very useful in optical trapping experiments as they allow direct elastic scattering spectroscopic measurements on a trapped particle, as already demonstrated for colloidal particles immersed in liquid [11], as well as other advantages in optical guiding [12]. Moreover, while the very wide optical spectrum allows the characterization of small spheres with large free spectral ranges and low resonance quality factors, optical trapping with a supercontinuum should open up enhanced techniques for the characterization of optical binding forces [13] along with the possibility of carrying out simultaneous trapping and spectroscopy with different parts of the spectrum.

In the present paper, we characterize the ability of a supercontinuum source to optically trap liquid aerosols. Specifically we explore salt water droplets in the size range from $3\mu m$ to $6\mu m$ in diameter. The droplets' dimensions are deduced from the elastically back-scattered spectrum which also allows us to examine droplet evaporation.

2. Experiment

The experiment uses an inverted microscope system similar to those previously used to optically trap airborne particles [3, 4, 14] and this is shown in Fig. 1. The light source is a linearly polarized 6W fibre laser pumped supercontinuum (Fianium SC450) of which a few tens of milliwatts are used. Only a fraction of the whole spectrum is used in our experiment, covering wavelengths from 650nm to 950nm. This can be considered as a "supercontinuum" given the size of the trapped droplets and as justified in the appendix B. The beam is expanded with a telescope consisting of achromatic lenses to overfill the microscope objective pupil (beam diameter $\simeq 8mm$). We use an infinity-corrected Nikon Plan Apochromatic (Numerical Aperture (NA)= 1.40) oil-immersion microscope objective. The beam is focused through a cover-slip covered by a $\sim 20\mu m$ water layer formed by falling aerosols in the trapping chamber. The paraxial focus is set 20μm above the water layer, a distance which we observed to be a good compromise between aberrations andthe probability to trap a droplet: the higher the focus, the more aberration but the larger the volume of the cone of light in air. The aerosols were produced by a Aerosonic® ultrasonic nebulizer. The initial solution is slightly doped with sodium chloride in order to decrease the droplet vapor pressure and reduce evaporation.
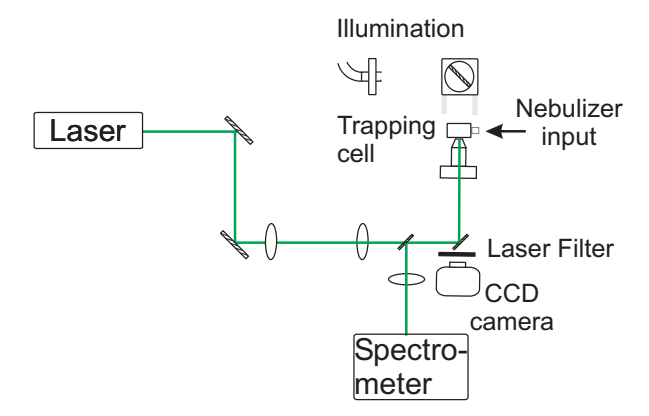

Fig. 1. Trapping experimental configuration. The light reflected on the trapped droplet is imaged on a spectrometer using a 70/30 beam-splitter.

The back scattered light is imaged both onto an Ocean Optics USB2000 fiber coupled spectrometer and, through dichroic filters, onto a camera. The trapped particle is illuminated from above with a fiber coupled halogen lamp (Thorlabs). Despite the set of dichoic filters, the visible part of the supercontinuum could not be filtered enough to get a sufficiently clear image to carry out video image sizing through the video image. Quantitative measurements were therefore achieved through spectroscopy.

On-axis light backscattered from a droplet produces a spectrum which exhibits fringes qualitatively corresponding to resonances of the Fabry-Perot (FP) interferometer made of the two opposite and concentric faces of the droplet (see Fig. 3). This analogy [15] is not exact in our case as the fringe contrast we obtain can be much larger than would be expected from such a FP interferometer. This inconsistency, as discussed in detail in the Appendix A and B, is due to the high numerical aperture of the focused beam.

Vector spherical harmonics form basis functions that may be applied to objects with a spherical symmetry such as droplets. The decomposition of focused Gaussian beams with this basis shows that the larger the numerical aperture, the smaller the number of excited modes [16, 17] at the focus. However, when the origin of the decomposition, centered on the sphere, is chosen

to be away from the focus, the number of excited modes increases (see Appendix A); far away from the focus the beam looks like a plane wave.

3. Droplet's radius determination

It is straightforward to deduce the size of the trapped droplet from the free spectral range of spectral fringes (see Fig. 3). However, the determination of the radius requires knowledge of the refractive index of the trapped droplet. The latter cannot be determined from the spectrum we obtain, contrary to the case of high orbital momentum TE and TM polarized whispering gallery resonances [18] in which relative position strongly depends on the index [19, 20]. It is thus impossible to measure a precise index value and we assume a value close to 1.33. As crystalline NaCl has a refractive index of 1.54, we estimate at saturation ($350g/L$), the index of an aqueous sodium chloride solution cannot exceed 1.35 which would account for a $\sim 2\%$ error. So while this method may be of poorer accuracy than those based on high-Q resonances, it may offer a better accuracy [21] than direct image measurement methods[14, 22].

To measure the droplet size, we choose the configuration where the fewest modes are excited so as to increase the fringe contrast and thus the accuracy of the measurement. This occurs at trapping intensities for which the droplet is the closest to the center on the paraxial focus of the beam. We show in Appendix B that for low orbital momentum modes, the free spectral range between resonances is given by:$\Delta\left(\frac{1}{\lambda_p}\right) = \frac{1}{4Na}$, where λ_p is the wavelength, p the resonance order, N is the index contrast of the droplet and a its radius. The droplets' radii were then measured by gathering the resonance peaks as fitted in Fig. 2.

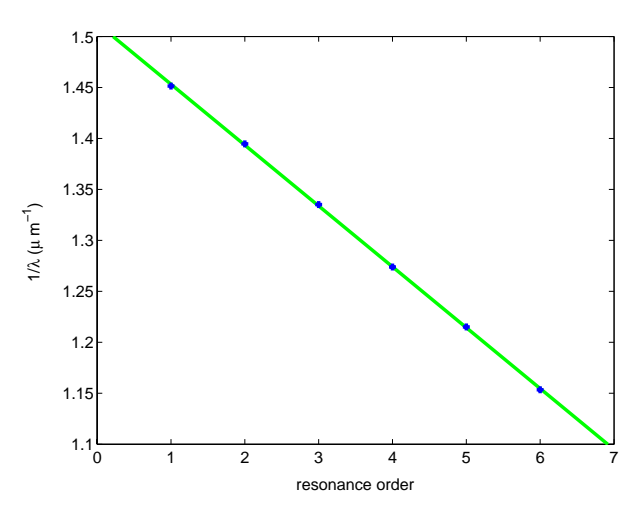

Fig. 2. Theoretical linear fit of resonances gathered for a $3.15\mu m$-radius droplet. The equation of the line is $\frac{1}{\lambda} = \frac{p_0 - p}{4Na}$ with $p_0 = 25.33$ and $4Na = 16.75$. For p_0 we would expect a integer plus $1/2$ from theoreticalmodelling but experimental incertainties do not enable such a precise value to be measured.

4. The effect of power on droplet trapping

At high trapping powers (high and low are relative terms based on the droplet size, see discussion related with Fig. 3 below), the droplet is centered on the focus of the trapping beam while at low power, it is trapped below the focus. In the former case, the spherical wave is reflected on the spherical face of the droplet, thus acting as a convex mirror. The resulting image

on the camera, set in the image plane of the paraxial focus, is a bright spot.

As we have already mentioned, when we vary the trapping power, the droplet height also changes along the beam axis which in turn alters the backscattered field. An example is shown in Fig. 3.
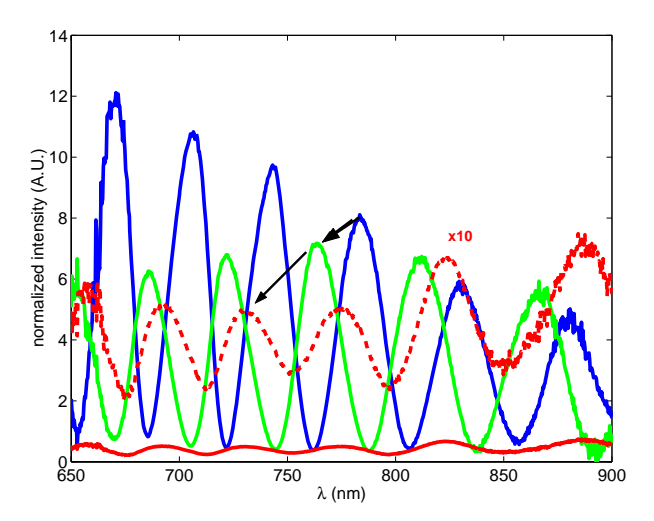

Fig. 3. Experimental normalized back-scattered spectrum coming from a droplet at three different trapping powers: $4mW$ (blue), $2mW$ (green), $1mW$ (red), $1mW$ $\times10$ scale enhanced (dashed red). The black arrows indicate the blue-drifting of peaks as the droplet is also evaporating during the experiment.

The droplet's z-coordinate decreases with the power so that the droplet probes the beam at different heights. Close to the focus, few modes are excited and the contrast of the spectral fringes is large; for low powers, the droplet sees a larger beam waist, the number of excited modes is larger and the contrast is degraded. So the droplet can still be sized as the height changes; just the fringe contrast changes. We discuss the contrast of fringes more extensively in Appendix B.

It was noticed that efficient trapping required the initial optical power be in a certain range (see Fig. 4). For powers lower than the lower limit of this range, the droplet is too heavy to be confined in the trap while for powers roughly four times as large, the droplet is ejected from the trap. This ejection suggests that absorption cannot be neglected implicating brownian radiometric forces [23] as being a factor or more plausibly that the droplet is not strictly speaking "tweezed" along the beam axis. The implication is that we are tweezing up to a certain intensity after which the scattering force overwhelms the gradient force. This is consistent with our previous observations of optically trapped aerosols using high NA optics. Theoretical calculations [24] considering monochromatic laser trapping of aerosols suggest for some droplet sizes and distances above the coverslip we are gradient beam trapping and for others we are radiation pressure trapping. It so happens that the combination of size, refractive index contrast [25] and optical setup used for high NA aerosol trapping is very close to the cross over regime where gradient forces dominate over scattering forces.

With experience, we could estimate accurately from the direct image on the camera, when the droplet was about to leave due to a too high intensity. In Fig. 4, the maximum trapping powers were recorded in this way. Then, the power was decreased until the droplet was lost, in order to estimate a longitudinal (axial) trapping efficiency defined as (where the refractive

index of air, $n_{air} = 1$):

$$Q = c\frac{F}{P}$$

where c is the velocity of light in air, F the optical force deduced from the weight compensation and P the estimated trapping power. The power at the trapping site is difficult to measure directly due, for example, to reflection from the cover-slip. In particular, measurement of trapping efficiency for air trapping experiments cannot use the usual two microscope objectives technique. For our calculation, we then measure the total intensity incident on the back of the microscope objective. The largest trapping efficiency was obtained for the largest trapped droplet and with Q estimated to be ~ 0.16, which with our overstimate of the trapping power is a lower limit on the trapping efficiency.
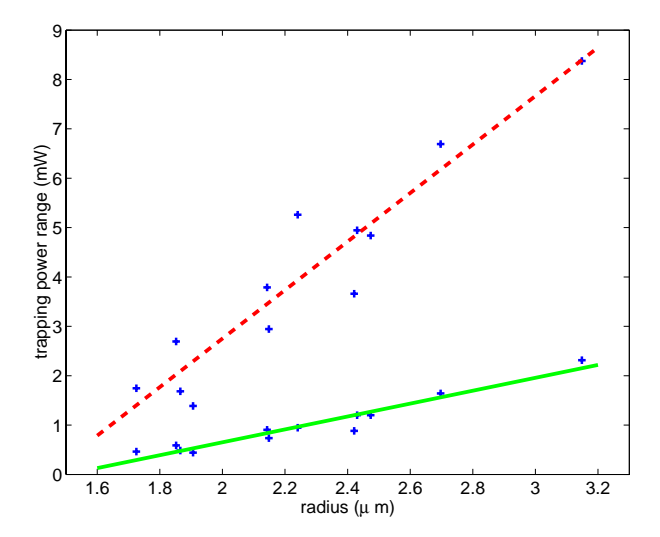

Fig. 4. Minimum and maximum trapping powers as a function of the radius of the water droplet. The red-dashed suggests that the optical force balance the weight. The green-solid line allows the calculation of a trapping efficiency along the axis. For the $\sim 3.2\mu m$ in radius droplet, the trapping efficiency is roughly 16%.

In Fig. 4, the lines are a numerical fit corresponding to the classical regime where the optical force does not vary with the size parameter of the droplet. Indeed, for large spheres, the scattering force is proportional to the square of the radius. The intensity balancing the weight (proportional to the cube of the radius) varies then linearly with the radius. A more accurate model should take Mie resonances (or Fabry-Perot resonances) into account. We argue that both the wide spectrum, covering several Fabry-Perot-typed resonances, and the low orbital momentum of excited modes contribute to smoothen resonance effects. High-Q resonances were described as radiation pressure spectroscopy in a pioneering optical levitation configuration [26].

From an experimental point of view, the interval between the two lines indicates the range of trapping power that must be used to trap water droplets as a function of their radius. As in our experiment the largest droplets are the end result of the merging of several smaller droplets (as they are unlikely to be made directly by the nebulizer), we had to increase the power while the trapped droplet grew in order for it to remain trapped. In the opposite case of evaporation (discussed in detail below) a reduction in the laser power is necessary to retain the droplet.

5.   Evaporation observation

As the droplet is trapped, it undergoes a rapid evaporation until an equilibrium size is reached. This is achieved by doping the droplets with sodium chloride. This has the effect of lowering the vapor pressure of the droplets and allowing them to reach an equilibrium size even in a subsaturated environment [4]. Such evaporation can be observed spectrally by noting the shift of fringes towards the blue region of the spectrum. Our experimental chambers do not have precise relative humidity (RH) control and it can take several seconds for humidity equilibrium to be reached. Another effect of this lack of RH control is that droplets can be observed to evaporate over longer timescales, mimicking behaviour which could otherwise be experimentally induced, to observe, for example, evaporation dynamics.

As trapping with the supercontinuum allows a direct and accurate determination of the droplet's size, it is possible, in particular, to study evaporation. Here, we present quantitative data showing the evaporation compared with a phenomenological exponential fit with a 1% agreement (see Fig. 5b). The precise modelling of evaporation critically depends on the relative humidity, which we cannot accurately determine in our experimental configuration (although optical tweezers methods can be employed to determine RH [27]).

The peaks obtained in the back-scattered spectrum slowly drift towards the "blue" region of the spectrum as seen in Fig. 5(a). The spectrum shown has been normalized by the impinging spectrum profile. The low recorded intensities on the edges of the spectrum around 650nm and 950nm do not allow a good normalization so that the exploitable spectrum only lies within the range $675nm - 900nm$.
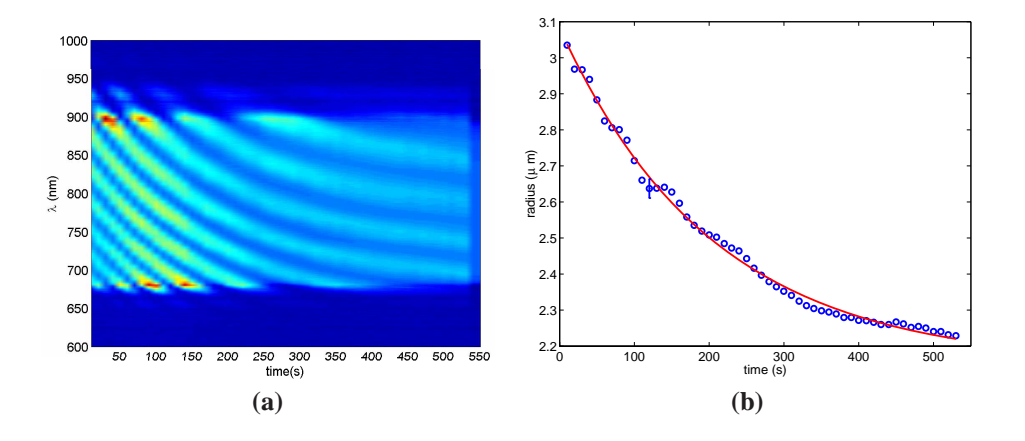

(a)   (b)

Fig. 5. (a) Color-coded back-scattered normalized spectrum coming from an evaporating salt water droplet. The spectrum is slightly blue-drifting with time. (b) Corresponding evolution of the radius obtained from the fit of the spectrum by a sine function. The evaporation is fitted with a exponential curve having a 205s decreasing time. An error-bar corresponding to a $\pm 1\%$ precision is added at 120s.

During the experiment, and after the droplet has reached an initial equilibrium size, the droplet's radius varies from $3.04\mu m$ to $2.22\mu m$. This long evaporation process lasted for a few minutes before the droplet, becoming too small, leaves the trap. Finally, we noticed that changing the intensity of the illuminating halogen lamp also displaced the equilibrium radius of the trapped droplet. We assume that in this case, the vapor pressure in the trapping cell is increased by the evaporation of the very lightly "salted" water layer on the cover-slip.

6. Conclusion

We have successfully demonstrated optical trapping of 3-6 micron diameter salt water droplets in air with a supercontinuum source, covering consistently several Mie resonances. The droplet radius could be accurately determined to $\sim 2\%$ thanks to the broad backscattered spectrum, limited by the uncertainty in the value of refractive index. Evaporation of the aerosol can also be followed. Our data suggests that trapping droplets at different heights will enable a precise probing of the trapping beam modal decomposition. These measurements could then be compared, for instance, to theoretical models of a beam focused through multi-layer interface (water and air, for example) [28]. Our results also suggest that the trapping of water aerosols can be interpreted as being more akin to optical levitation than to optical tweezing.

The use of a supercontinuum source for probing droplets may also enable the use of the extended spectrum to trap with one wavelength and carry out spectroscopy or fluorescence excitation and imaging with another, offering new optical imaging capabilities to interrogate airborne particles.

Acknowledgements

A. Focused beam: multipolar description

The beam focused in air, in the trapping chamber, has a numerical aperture exactly equal to 1 as the back aperture of the microscope objective is illuminated through total internal reflection at the glass coverslip. We assume the water layer on the coverslip improves the transmission coefficient as it has an refractive index between that of glass and air. The focused beam is also strongly aberrated as the microscope objective has been designed to minimize aberrations when imaging on the surface of a coverslip. The second effect introduced by the water/air interface is on polarization. As TE and TM polarized modes incident on the coverslip have different transmission coefficients, the focused beam loses its rotational symmetry pasing through the objective.

Nevertheless, this appendix is not intended to rigorously model our optical system but to give a theoretical insight into the experimental results. We will then suppose to simplify arguments that the beam has a revolution symmetry.

A focused x-polarized beam with a rotational symmetry for a dielectric sphere on its axis can be expressed as the sum of its angular spectrum plane wave decomposition. Every plane wave can then be expanded on vector spherical harmonics (only azimuthal numbers $m = 1$ modes are excited) [16]:

$$\mathbf{E} = \sum_n G_n E_n (\mathbf{M_{o1n}} - i.\mathbf{N_{e1n}})$$

Where $E_n = i^n \frac{2n+1}{n(n+1)}$ and

$$G_n = \int_0^\pi [\cos(\theta)]^{1/2} \sin(\theta) d_{1,1}^n(\theta) g(\theta) \exp[ikz\cos(\theta)] d\theta$$

with g being the beam profile in the angular domain (corresponding to the Fourier domain in paraxial optics) and $d_{1,1}^n(\theta)$ being the rotation vector of $m = 1$ spherical harmonics[29]. k is the beam wavevector and z the longitudinal propagation co-ordinate.

The radial parts of the vector spherical harmonics **M** and **N** are given by the spherical bessel function of the first kind. G_n would be uniformly equal to one for a plane wave (g is a Dirac delta function) and vanishes for large n's when the function g is wide. For a non-aberrating Gaussian beam with a $NA = 1$, the typical number of excited modes is ~ 5 at the focus point. G_n becomes uniform far away from the beam focus where the waist of the beam becomes large compared to the considered scattering sphere and looks like to a plane wave.

B.   Backscattered field

When the radius of the sphere of radius a and index N is large compared with the wavelength, the droplet can be modelled as a Fabry-Perot interferometer[15] with a free spectral range equal to $\Delta\left(\frac{1}{\lambda_p}\right) = \frac{1}{4Na}$. However, the finesse we obtain experimentally (see Fig. 3) is much bigger than in the classical case ($\sim 1\%$ for 1.33 index contrast) mainly because only a few modes are excited. This case requires then more a deeper theoretical treatment.

For a sphere illuminated by the beam described by the formula given in Appendix A, the backscattered far field on the propagation axis can be derived:

$$\mathbf{E}_\infty(\theta = \pi) = i\frac{\exp(ikr)}{kr}\mathbf{x}\sum_{n\geq 1} G_n\left(n+\frac{1}{2}\right)(a_n - b_n) \tag{1}$$

Where a_n and b_n are Mie scattering coefficients as defined in ref [30]. As only a couple of modes are excited in a droplet in the vicinity of the focus, we can develop $a_n - b_n$ in the particular case $n \ll Nka$ (k being the wavenumber):

$$a_n - b_n = i(-1)^{(n+1)}\exp(-2ix)\frac{\sin(2Nx)}{\alpha\cos(2Nx) - i\sin(2Nx)} \tag{2}$$

with

$$\alpha = \frac{2N}{N^2 - 1}$$

We notice that this expression depends on the mode number only in its sign and then, the periodic part of it can be factorized in the former expression of the backscattered field. If we now take the intensity, the resonating wavelength satisfies:

$$4N\frac{a}{\lambda_p} = \frac{1}{2} + p$$

where p is an integer. The physical meaning of the $+1/2$ is the Gouy phase shift introduced by the focusing of the mode between the two spherical mirrors in the Fabry-Perot model. Consequently, the free spectral range is:

$$\Delta\left(\frac{a}{\lambda_p}\right) = \frac{1}{4N}$$

as in the case of the Fabry-Perot model. This formula is only valid for $n \ll Nka$. For larger n, numerical simulations indicate that $a_n - b_n$ is shifted toward "red" wavelengths. This shift, difficult to express analytically, does not significantly further aid our understanding of the physics in this discussion. However, for an increasing number of excited modes, these shifts degrade the contrast of the spectral fringes.

It is interesting to compare this result to the oscillations of trapping efficiency[31] and equilibrium position[16]. Although the back scattered intensity corresponds to reflected optical momentum, we do not see any simple quantitative connecting formula between the back scattered intensity and the trapping efficiency. However, it appears that both trapping efficiency[31] and

equilibrium position[16] have the same oscillation period with the size parameter. We identify here the key argument to say the spectral width of the laser appears as a supercontinuum for the droplets we trap as the spectrum always covers several units of *Nka*. The optical gradient force is then averaged over all these oscillations.

Finally, our assumptions are based on the fact that the oscillations of the spectrum we describe are due to a few low orbital momentum numbers and must not be confused with usual whispering gallery resonances observation which involves several high orbital momentum number modes.